ФИЗИЧЕСКИЕ ПРИБОРЫ ДЛЯ ЭКОЛОГИИ
МЕДИЦИНЫ, БИОЛОГИИ

ON GAMMA-RAY SPECTROMETRY PULSES REAL TIME DIGITAL SHAPING AND PROCESSING

© 2011 г.   B. Boghrati, A. Moussavi-Zarandi, V. Esmaeili-Sani, N. Nabavi, M. Ghergherehchi

Faculty of Physics, Amirkabir University of Technology
424, HafezAve, Tehran, Iran

In gamma-ray medical imaging and nuclear spectroscopy instruments, deployment of high speed reconfigurable field programmable gate arrays circuits make it possible to implement signal processing algorithms for pulse shaping, pile up detection and correction, and determination of pulse amplitude and its time of detection in real time. Based on this idea, we have developed a digital pulse processing board for use in a gamma ray spectroscopy and later in positron emission tomography. The proposed digital pulse-processing core relies on digital trapezoidal or triangular pulse shaping, an automatic baseline correction and pileup rejection methods, all of which are implemented in FPGA to permit on-line event processing. Experimental results show that because of its pulse shaping method, system throughput and energy resolution significantly outperforms analog pulse processing systems.

1. INTRODUCTION

The traditional function of a gamma spectroscopy system consists of converting the electrical-charge pulses from the detector into current or voltage pulses and obtaining their amplitude distribution function [1]. Pulse shaping and noise filtering is accomplished by digital signal processing (DSP) integrated circuits [2–5]. This permits a wider range of available shaping parameters, and hence provides the possibility of selecting the settings for optimum resolution and/or throughput for a detector [4].

The shape may be of particular interest in high-count rate detectors where the identification and recovery of pileup events is essential [6]. Shape analysis is also a valuable technique to distinguish between different scintillator materials in special phoswich arrangements. In imaging applications such as PET, this may be utilized to determine the depth of interaction (DOI) [7–10]. On the other hand, the precise pulse starting time is essential for time-of-flight applications or coincidence detection [11].

In this paper, a brief description of the design of a digital signal processing board for a gamma spectrometer will be given. Experimentally, we have benchmarked our DSP performance by comparing its throughput and energy resolution to those from MCA systems presented in references [12–18], and future prospects are discussed. Also, our studies are motivated by the development of a new PET scanner where information for energy discrimination, coincidence detection, event localization and optionally DOI determination is needed.

2. DIGITAL SIGNAL PROCESSING BOARD ARCHITECTURE

The first step for on-line pulse processing is using high-speed analog to digital converter. In this condition, a straightforward digitization method is to use a free-running ADC [19].

In order to preserve the detailed shape of input signal, the fast sampling ADC operates currently at 65 MHz. The acquired digital samples hold the information of interest so there is no need for further analog hardware such as discriminators, shaping or coincidence detection circuits and hardware pulse-shape analyzers [20].

Under these conditions, all of the necessary signal processing must be done by implemented algorithms in the FPGA. The digital signal processing board has been designed with this purpose. Fig. 1 shows the block diagram of the digital gamma spectrometer. The main block of the digital data acquisition board consists of: 1) amplifier and anti-alias filter to satisfy the Nyquist condition; 2) high speed ADC digitizer; 3) hgh speed Master DSP used for digital pulse shaping, filtering and analysis programmed in FPGA; 4) high speed ARM DSP controller for monitoring and controlling the entire system and data communication with the main station or PC for data reconstruction.

We used an AD9235 12–bit ADC, which provides low power consumption (320 mW) and a sampling rate up to 65MSPS [21]. The low values of differential and integral non-linearities are other important specifications of this inexpensive device. The digital data output of the ADC is sampled at 65 MHz and passed to the Xilinx FPGA (XC3S400) [22]. At this stage, the
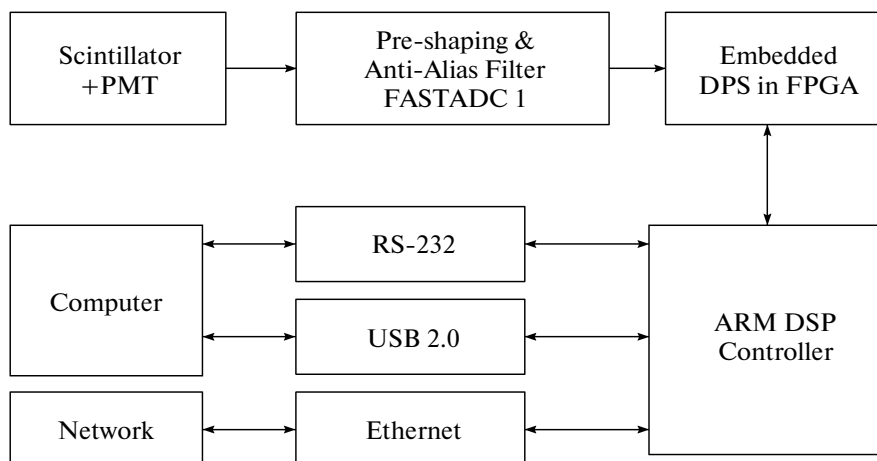
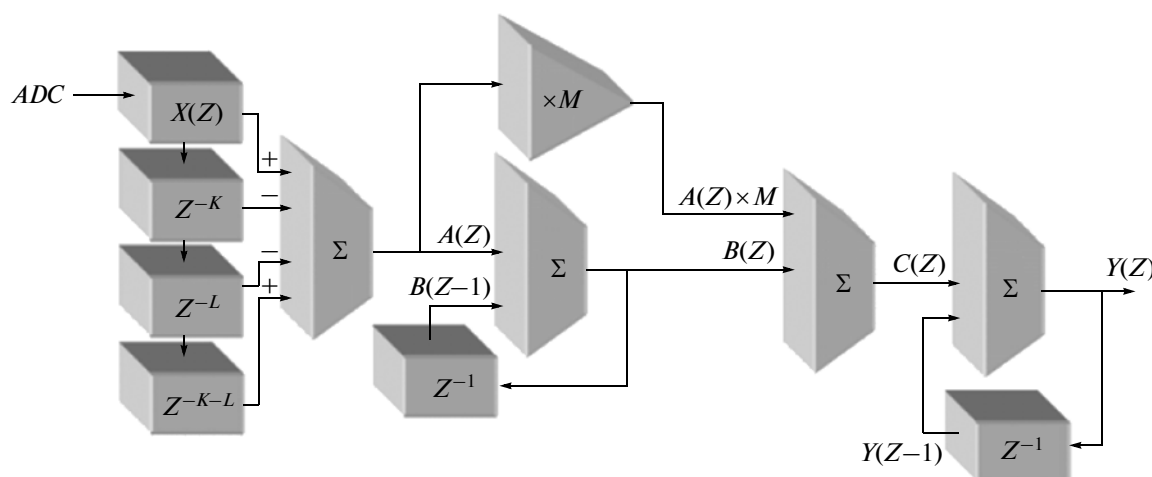**Fig. 1.** Block diagram of digital data acquisition system.

Fig. 2. Digital Trapezoidal/Triangular Filter.

digital samples are processed with a digital filter algorithm to convert the sampled input signals into trapezoidal or triangular waveforms [23–31].

After signal processing, the detected event energy peak and time of its occurrence are stored in fast SRAM for further processing such as histogram reconstruction in gamma spectroscopy. We implement the histogram reconstruction algorithm in the FPGA and send its results to the next stage, i.e. the ARM DSP, to transmit it to the main station or PC.

The recursive algorithm that converts a digitized exponential pulse $X(n)$ into a symmetrical trapezoidal pulse $Y(n)$ is depicted in Fig. 2 [23–25]. X, A, B and Y are equal to zero for $n < 0$. The parameter M depends only on the decay time constant τ of the exponential pulse and the sampling period T_{CLK} of the digitizer, and is given by $1/\left(e^{T_{CLK}/\tau} - 1\right)$. Under such circumstances, the duration of the rising (falling) edge of the trapezoidal shape is given by the smaller value of K and L, $(\min(k, l))$, and the duration of the flat top of the trapezoid is given by the absolute value of the difference between K and L, $(abs(t - k))$.

This unit is implemented in the FPGA and performs pulse shaping every time the ADC samples more than the low-level threshold. In this condition, the digital trapezoidal/triangular pulse shaper has enough time to complete its process. It must be mentioned that the final speed of pulse processing in an FPGA depends on the complexity of code construction and the optimization type of synthesis software. We are using the Xilinx ISE and set its optimization process to the timing optimizer. The final speed of the pulse processor after synthesis completion is about 76 MHz. The digital resolution of the accumulators should be sufficient to accommodate the maximum possible digital value of the output data, so we set all pulse processor constructions to the 32 bit.
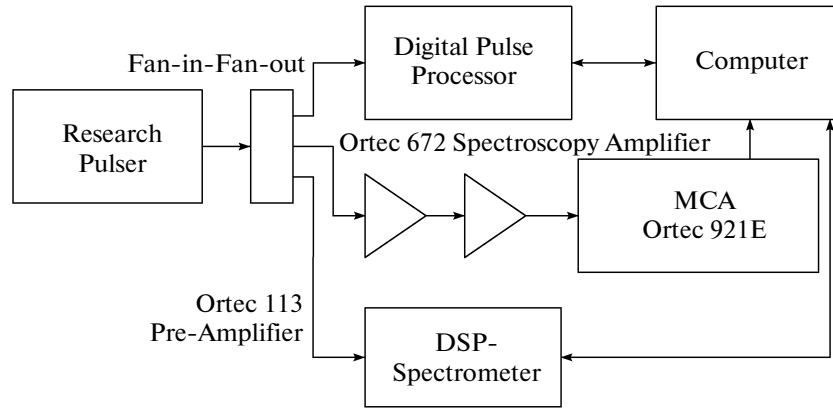
Fig. 3. Experimental setup for Digital Pulse Processing (DPP) performance evaluation.

3. EXPERIMENTAL SET UP

Several tests were conducted to verify proper functioning of the digital pulse processor and to characterize its performance. As a primary test for surveying the DSP pulse processing algorithms and precise comparison between our DPP board performance and the

Digital desktop spectrometer Polaris [32, 33] and Ortec spectrometer [34], we used the setup shown in Fig. 3. In this case, we used the BNC-BP5 research pulser to reduce input pulse noise and some non-linearity of input signals originating from the statistical uncertainty of a detector. This condition exhibits noise
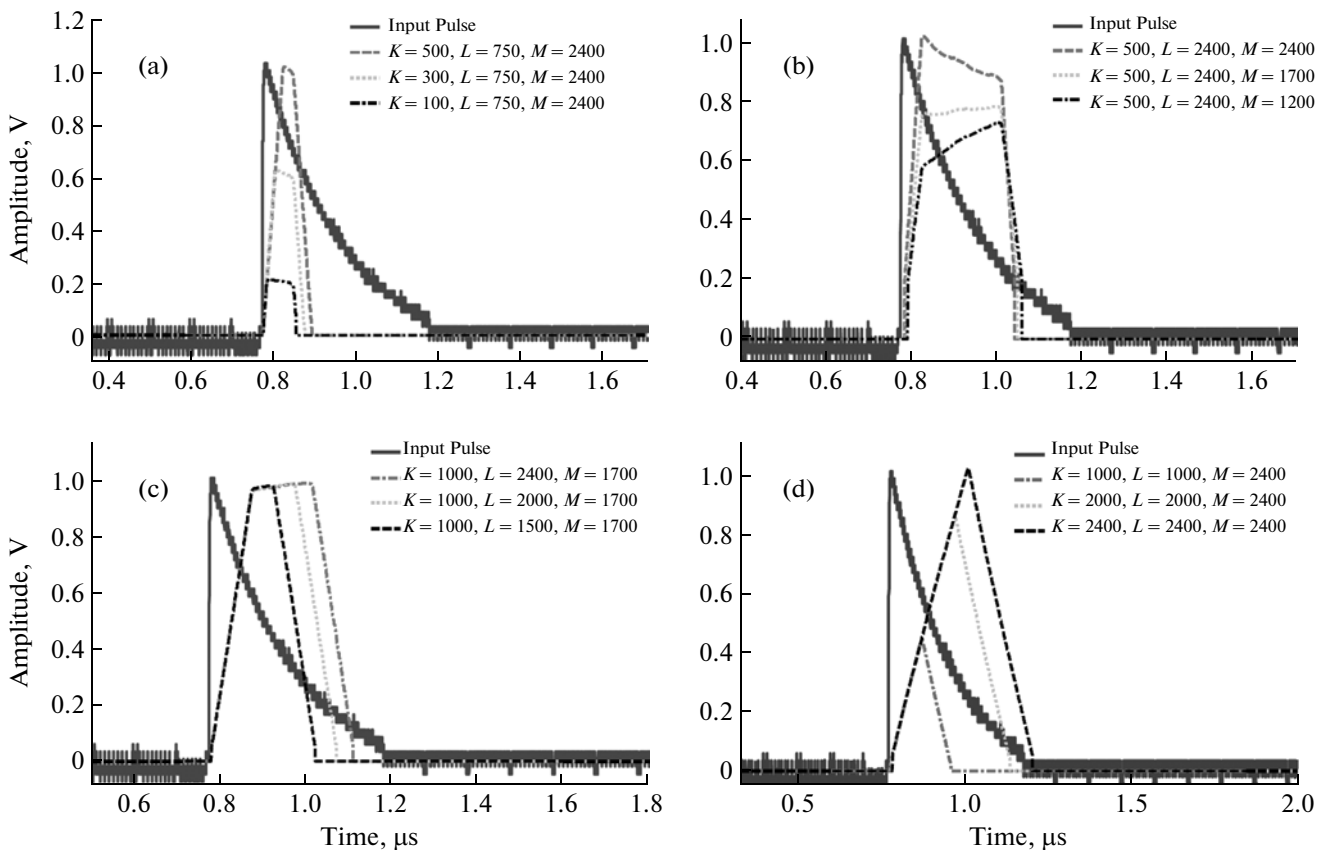

Fig. 4. Output pulse shapes response of trapezoidal/triangular digital filter algorithm to the input impulse signal: (a) the effect of change of parameter K on trapezoidal pulse height; (b) the effect of change of parameter M on trapezoidal flat top duration; (c) the effect of change of parameter L on trapezoidal pulse durations; (d) the effect of change of parameters K and L when they have equal values.
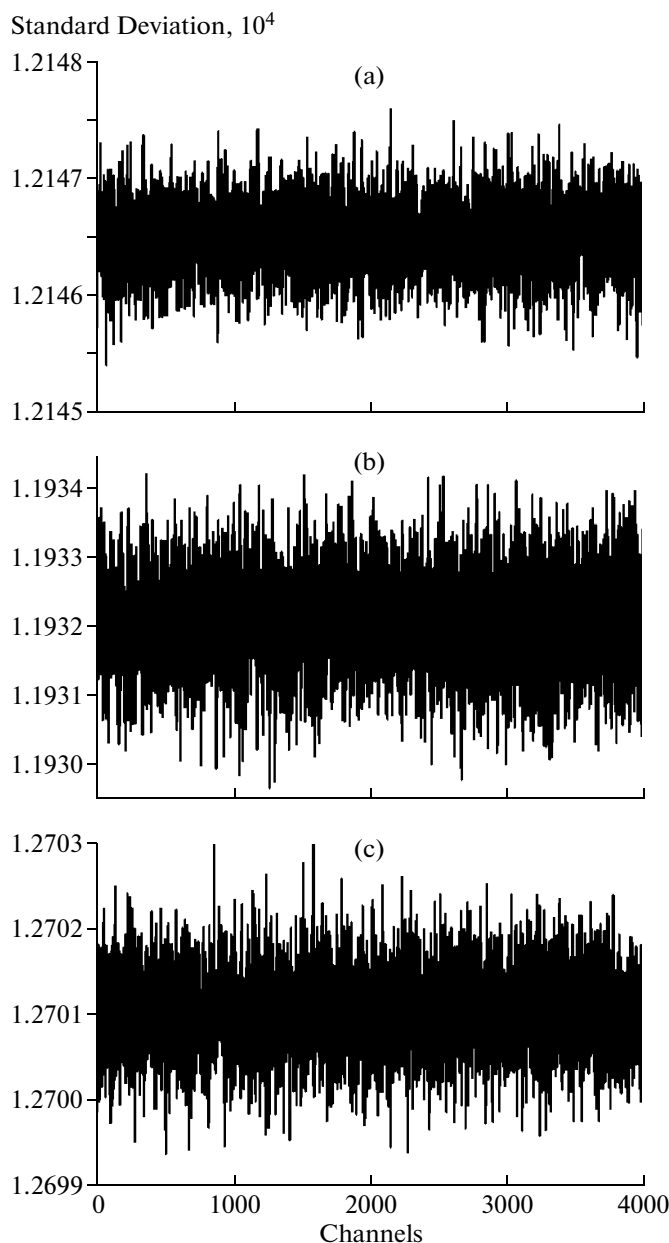
Standard Deviation, 10^4

Deviation, channels

Fig. 6. Integral non-linearity as a function of centroid location.

Fig. 5. Differential non-linearity errors of: (a) DSP1, (b) DPP, (c) NIM.

and other non-linearity errors of the electronics. In the second step, by applying the ramp pulses to the pulse processor unit we were able to extract the exact value of the overall differential non-linearity of each system.

Finally, to study the behavior of our DPP when the other sources of noise are added into the input signals, a NaI detector was used and irradiated by ^{137}Cs. The activity of this source was about 350 kBq. We adjusted the distances between source and detector so that the input count rates ranged from 10^4 counts/s for energy
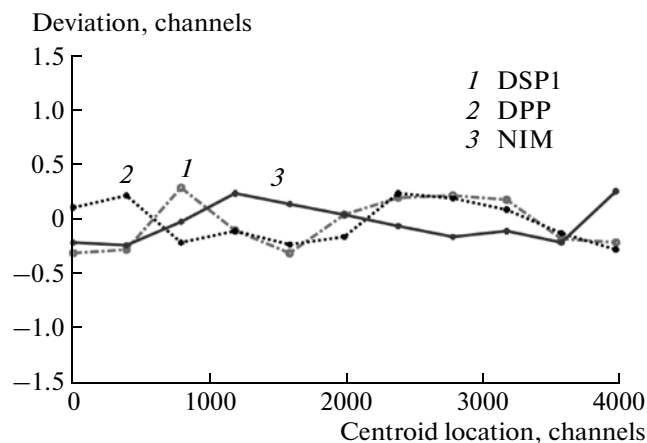
resolution evaluation to about $12 \cdot 10^4$ counts/s for maximum throughput evaluation.

The pulse processors system behaviors were evaluated with two different settings. For a very high throughput scenario, we set both the rise time and the flat top of the trapezoidal filter function to 0.625 μs; i.e. 1.2 μs triangular pulse shaping. This value is the minimum practical value for our digital pulse processor and digital desktop pulse processor. The previous studies have indicated that such a setting seems to maximize the throughput [28−31]. Also based on previous studies, for a good resolution scenario, we set the rise time to 5.6 μs and the flat top to 0.8 μs; i.e. 12 μs trapezoidal pulse shaping. The Ortec system was also evaluated with two settings, both in the triangular mode. For a high−throughput scenario, we set the shaping time to 0.5 μs, and for a normal, good resolution scenario, we set the shaping time to 6μs based on the manufacturer's recommendation.

4. RESULTS AND DISCUSSION

4.1. General aspects

The observed digital output pulse shapes transferred from the DSP system to the computer are shown in Fig. 4. As Fig. 4a shows, increasing K from 100 to 300 and 500 leads to a change in the amplitude of the pulse and a smaller effect on pulse duration, so K can be used for pulse height control in digital pulse shaping algorithms. Increasing M from the values of 1200 to 1700 and 2400 skews the flat top of the trapezoidal pulse, as shown in Fig. 4b, so this factor determines the tilt of the trapezoidal pulse. On the other hand, Fig. 4c shows that a change of L from 1500 to 2000 and 2400 increases the pulse width duration T_p and flat top duration T_{top}. Under these conditions, any change of L values has no significant effect on the

Energy Resolution, keV

Output Count Rate, $10^4\,\text{s}^{-1}$

Input Count Rate, 10^4 counts/s
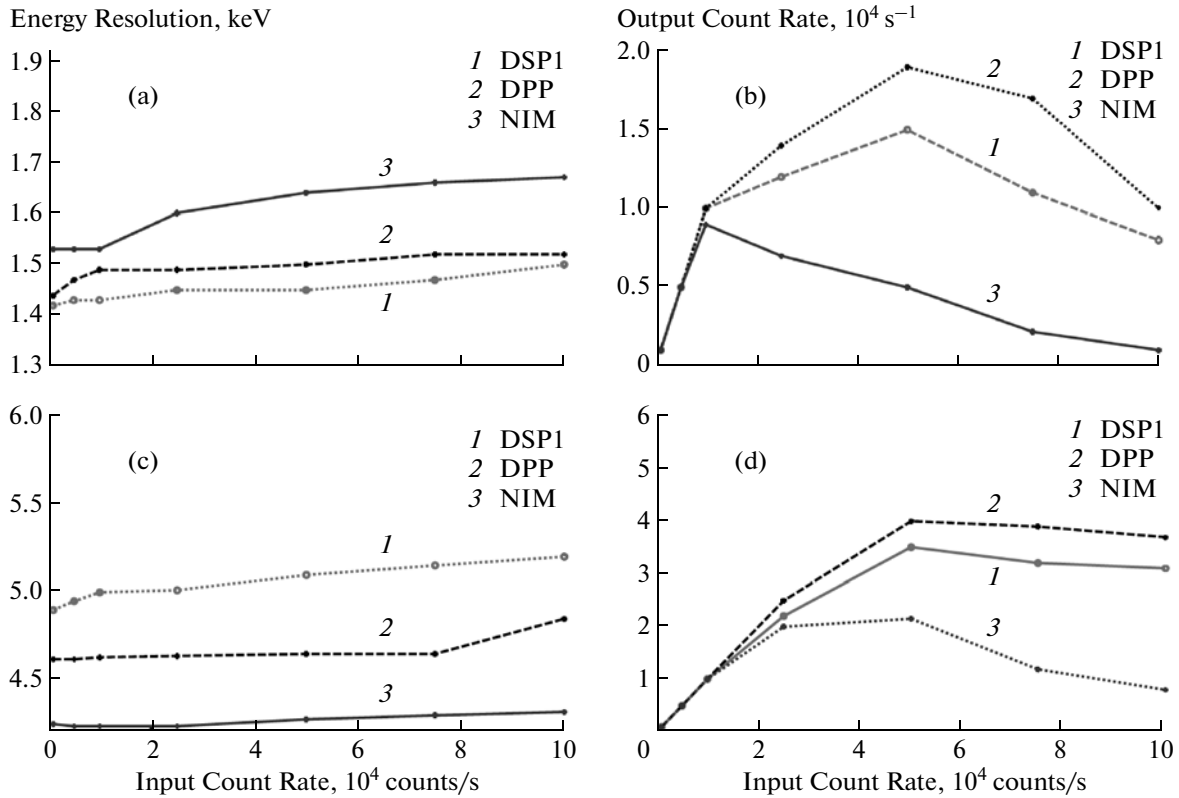
Fig. 7. Energy resolution and output count rate at 662 keV as a function of input count rate for two shaping time ($2t_{rise} + t_{flattop}$): (a) Energy resolution at long shaping time DSP1 and DPP = 12 µs and NIM = 5 µs; (b) Output count rate at long shaping time DSP1 and DPP = 12 µs and NIM = 5 µs; (c) Energy resolution at short shaping time DSP1 and DPP = 1.2 µs and NIM = 0.5 µs; (d) Output count rate at short shaping time DSP1 and DPP = 1.2 µs and NIM = 0.5 µs.

pulse amplitude. When $K = L$ (Fig. 4d), trapezoidal pulses change to triangular pulses.

The pulse shaping time in digital systems is defined as:

$$t_p = t_{rise} + t_{fall} + t_{flattor},$$

so when the triangular pulse shaping is used instead of trapezoidal form, the final pulse shaping time is reduced to

$$t_p = 2t_{rise} = 2t_{fall}.$$

The chance of pulse pile-up is reduced with narrower output pulses, leading to a higher potential count rate. When the input count rate is high, it is better to use a triangular pulse shape to reduce the output pulse width and reduce the pulse pile-up effects: the flat top duration T_{top} approaches zero and the pulse rise and fall times change equally, based on the value of K or L. In our design, all of these parameters are digitally controlled by internal control logic and the ARM DSP controller.

4.2. Differential Non-Linearity error

As mentioned in the previous section, by applying the ramp pulses it is possible to calculate the overall differential non-linearity of each pulse processor system. By using the resulting histogram as shown in Fig. 5, the differential non-linearity was calculated for each channel, following [18, 21]:

$$DNL_n = [H_n/(M \times P_n) - 1] \cdot 100,$$

where $DNLn$ represents the differential non-linearity of channel n as a percentage of one least significant bit (LSB); Hn represents the number of counts recorded in channel n; M represents the total number of counts contained in all channels; P_n represents the probability of channel n containing a count. P_n would ideally be the reciprocal of the number of channels containing counts. The DNL thus obtained for our digital pulse processor (DPP), desktop pulse processor spectrometer Polaris and Ortec spectrometer were respectively ±0.27%, ±0.25% and, ±0.33%.

The inexpensive ADC (AD9235) has more DNL than its counterpart in the Digital desktop spectrometer (AD6644), so the differential non-linearity of our DPP is slightly more than that of the Digital desktop spectrometer. The Ortec system appears to possess some differential non-linearity, but it is also very small.

4.3. Integral Non-Linearity error

The integral non-linearity of each pulse processor was obtained by applying 10 known evenly spaced magnitudes from channel 10 to channel 4000. The degree to which the resulting peak centroid deviates from the best straight-line fit of the resulting data determines the amount of INL. Fig. 6 presents a graph of the integral non-linearity of the pulse processors versus centroid channel number as determined by a straight-line fit applied to the data.

4.4. Optimized Resolution and Throughput

For final comparison of the pulse processors system performance, we evaluated their throughputs with two different setting as mentioned before. In this case, input count rates varied from 1000 to 100 000 counts/s for the high throughput measurements and for the good resolution measurements.

Observed throughput rates for each of the two scenarios are summarized in Fig. 7. As shown in Fig. 7a for an NaI detector at lower input count rates up to 10^5 counts/s, the energy resolution of our digital pulse processor (DPP) and the desktop DSP spectrometer Polaris (DSP1) are the same and significantly better than that of the Ortec (NIM) pulse processor. The output count-rate values of the two digital systems are approximately two times better than the Ortec throughput when the pulse shaping is set for optimized energy resolution. Normally the long shaping time would give better resolution than the short shaping time at low count rate. However, the large shaping times are more susceptible to electronic noise effects. A system with large electronic noise effects may require a short shaping time for the best performance. This is evidence that the Ortec system has unusually large electronic noise effects, which degrade its energy resolution when the filter pulse shaping is set to a large value. On the other hand, when the three systems are set to optimized throughput condition, the maximum throughput of digital pulse processor and digital desktop spectrometer are increased to about $5 \cdot 10^4$ counts/s.

There is the same situation for an Ortec pulse processor system, i.e. its maximum throughput increases two times relative to the energy-optimized condition. However, the effects of decrease of pulse shaping are more remarked in the two digital systems as mentioned earlier.

5. CONCLUSIONS

In this work we have designed a digital pulse processing board for using in a gamma ray spectroscopy or with some modification in PET scanner imaging. The number of analog circuits is minimal, because the whole processing scheme is accomplished in the digital domain. The central part of the system, the high-speed pulse processor, is realized using an FPGA device. The main parameters of the system performance, i.e. differential and integral non-linearity errors, optimized energy resolution and system throughputs are investigated and compare favorably with commercial digital desktop spectrometer and analog spectrometer systems.

Results of these experiments show that fully integrated electronics and fully integrated pulse processing chain into the FPGA make the DPP fully protected against electronic noise and comparable with the standard low noise digital and analog pulse processing systems. The other sources of non-linearity errors in the design DPP are as low as in the counterparts. It is possible to change the behavior of the system from optimized energy resolution to optimized throughput rate by changing the filter characteristics. The optimized energy resolution and throughput observed for designed DPP appear to be the same as digital desktop spectrometer in various ranges of input count rates. Overall, the system performance comparisons show that the designed DPP is fully reliable for using in real time gamma spectroscopy, prompt gamma analysis or future design steps in a PET scanner.

REFERENCES

1. Knoll G.F., *Radiation Detection and Measurement*, third ed., New York: Wiley, 2000.
2. Jordanov V.T., *IEEE Trans. Nucl. Sci. Symp.*, 1999, vol. 1, p. 375.
3. Polushkin V., *Nuclear Electronics, Superconducting Detectors and Processing Techniques*, New York: John Wiley & Sons , 2004.
4. Dryak P., *Applied Radiation and Isotopes*, 2004, no. 60, p. 203.
5. Xiao W., *NucI. Instrum. and Methods A*, 2005, vol. 555, p. 231.
6. Kafaee M., *NucI. Instrum. and Methods A,* 2009, vol. 607, p. 652.
7. Inadama N., *IEEE Trans. Nucl. Sci.*, 2002, vol. 49, no. 3, p. 629.
8. Barbier R., *NucI. Instrum. and Methods A,* 2004, vol. 527, p. 175.
9. Moses William W., *NucI. Instrum. and Methods A,* 2001, vol. 471, p. 209.
10. Simon A., *NucI. Instrum. and Methods A,* 2005, vol. 546, p. 33.
11. Leroux J.-D.,Tetrault M.A., Rouleau D., et al., *IEEE Trans. Nucl. Sci.*, 2004, vol. 56, p. 588.
12. James W.D., Raulerson M.R., *J. Radioanal. Nucl. Chem.*, 2001, vol. 248, no. 2, p. 283.
13. Koskelo M.J., Sielaff W.A., Hall D.L. et al., *J. Radioanal. Nucl. Chem.*, 2001, vol. 248, no. 2, p. 257.
14. Szentmiklósi L., Belgya T., Révay Zs., Molnár G.L., *J. Radioanal. Nucl. Chem.*, 2005, no. 1, p. 229.
15. Koskelo M.J., Koskelo I.J., Siela B., *NucI. Instrum. and Methods A,* 1999, vol. 422, p. 373.

16. Mitra S., Wielopolski L., Hendrey G., *Appl. Radiat. Isot.*, 2004, vol. 61. p. 1463.

17. Reguiguia N., Morelb J., Ben Kraiema H., Mahjoub A., *Appl. Radiat. Isot.*, 2002, vol. 56, p. 93.

18. Pauly S.W., *NucI. Instrum. and Methods A,* 1999, vol. 422. p. 379.

19. Streun M. et al, *IEEE Trans. Nucl. Sci.*, 2001, vol. 43, p. 524.

20. Lerche C.W., *IEEE Trans. Nucl. Sci.*, 2005, vol. 52, no. 3. p. 560.

21. Analog Devices Inc., available on the internet: http://www.Analog.com

22. Xilinx Inc., available on the internet: http://www.Xilinx.com

23. Jordanov V.T., and Knoll G.F., *NucI. Instrum. and Methods A*, 1994, vol. 345, p. 337.

24. Jordanov V.T., Knoll G.F., Huber A.C., Pantazis J.A., *NucI. Instrum. and Methods A*, 1994, vol. 353, p. 261.

25. Georgiev A., and Gast W., *IEEE Trans. Nucl. Sci.*, 1993, vol. 40, no. 4, p. 770.

26. Grzywacz R., *NucI. Instrum. and Methods B*, 2003, vol. 204, p. 649.

27. Stein J., Scheuer F., Gast W., Georgiev A., *NucI. Instrum. and Methods B,* 1996, vol. 113, p. 141.

28. Radeka V., *IEEE Trans. Nucl. Sci.*, 1968, vol. 40, p. 455.

29. Cisotti M., de la Fuente F., Manfredi P. F., et al., *NucI. Instrum. and* Methods, 1979, vol. 159, p. 235.

30. Goulding F.S., *NucI. Instrum. and Methods A*, 1972, vol. 100, p. 493.

31. Jordanov V.T., *NucI. Instrum. and Methods. A*, 1994, vol. 351, p. 592.

32. Warburton W.K., Momayezi M., Hubbard-Nelson B., Skulski W., *Applied Radiation and Isotopes*, 2000, vol. 53, p. 913.

33. XIA Inc., POLARIS specification is available on the internet: http://www.XIA.com

34. Ortec Modular Pulse−Processing Electronics Catalog, www.ortec−online.com